JACS
JOURNAL OF THE AMERICAN CHEMICAL SOCIETY
Article
pubs.acs.org/JACS

Hopping-Mediated Anion Transport through a Mannitol-Based Rosette Ion Channel

Tanmoy Saha,[†] Sathish Dasari,[†] Debanjan Tewari,[§] Annamalai Prathap,[‡] Kana M. Sureshan,[‡] Amal K. Bera,*[,§] Arnab Mukherjee,*[,†] and Pinaki Talukdar*[,†]

[†]Department of Chemistry, Indian Institute of Science Education and Research Pune, Pune, Maharashtra 411008, India

[‡]School of Chemistry, Indian Institute of Science Education and Research Thiruvananthapuram, Thiruvananthapuram, Kerala 695016, India

[§]Department of Biotechnology, Indian Institute of Technology Madras, Chennai, Tamil Nadu 600036, India

Supporting Information

ABSTRACT: Artificial anion selective ion channels with single-file multiple anion-recognition sites are rare. Here, we have designed, by hypothesis, a small molecule that self-organizes to form a barrel rosette ion channel in the lipid membrane environment. Being amphiphilic in nature, this molecule forms nanotubes through intermolecular hydrogen bond formation, while its hydrophobic counterpart is stabilized by hydrophobic interactions in the membrane. The anion selectivity of the channel was investigated by fluorescence-based vesicle assay and planar bilayer conductance measurements. The ion transport by a modified hopping mechanism was demonstrated by molecular dynamics simulation studies.

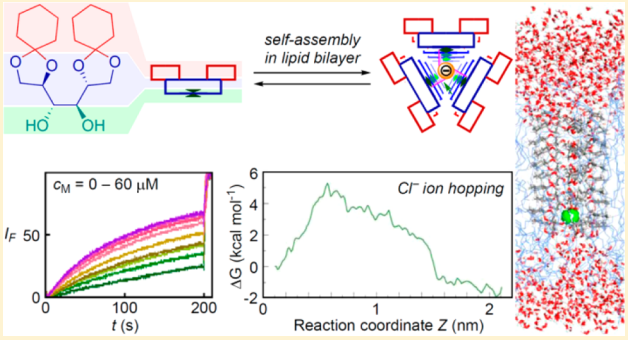

1. INTRODUCTION

The transport of ions across biological membranes is facilitated by a certain class of complex channel-forming proteins.[1−3] This process is essential for diverse biological functions such as sensory transduction,[4] cell proliferation,[5,6] and osmotic stress response.[7] In these channel-forming molecules, a number of ion-recognition sites are often disposed of along the narrow pore and the ions hop from one binding site to the next in single-file as the permeation proceeds.[8−10] Natural ion channels allow the passage of a particular ion and the selectivity is primarily governed by the strength of ion binding at these sites.[11−14] Therefore, the design of synthetic ion channels with repeating ion binding sites has been of significant interest.

In the majority of reported synthetic ion channels, a well-defined ion-recognition site is either absent or present only at a single position along the pore.[15−21] Synthetic ion channel design strategies for incorporating multiple ion-recognition sites have primarily resulted in cation selectivity. In 1999, Matile and co-workers reported a ligand-assembled ion channel in which two hepta(*p*-phenylene) units provided arrays of cation−π interaction motif in a single file (Figure 1A).[22] In this ion channel, a sandwiched binding motif involving two phenyl rings and a cation is repeated along the channel direction. The carbonyl−cation interaction motif has been used extensively in the design of cyclic peptide-based nanotubes (Figure 1B).[23−28] An alternate strategy to capitalize on the carbonyl−cation interaction was adapted in the construction of rosette-type molecules (Figure 1C).[29−31] Crown ether−cation interactions, a common cation-recognition motif,[32,33] was adapted by Winum and Matile,[34] Fyles and co-workers,[35] and Boudreault and Voyer[36] to construct hydraphile pores (Figure 1D). Self-assembled "barrel-stave" ion channels were constructed via the tethering of either vicinal diols or peptide side chains to a *p*-octiphenyl rod (Figure 1E).[37−40] However, these supramolecules were also cation selective.

Only the successful design of transmembrane supramolecules with single-file multiple anion-recognition sites were demonstrated primarily by Matile and co-workers. Oligonaphthalenediimide[41,42] and oligoperylenediimide[43] based rigid-rod molecules were reported to form π-slides in lipid vesicles. The selectivity of these supramolecules during ion transport studies were accounted for by anion−π interactions at each recognition site along the channel direction (Figure 1F). However, the single channel conductance data of these molecules are not available.

Therefore, the design of an anion selective artificial ion channels with multiple ion-recognition sites is still a challenge. In the pursuit to develop a robust ion channel system in spherical as well as planar bilayers, we looked into different anion-recognition motifs routinely applied in anion binding. The abundance of hydroxyl (−OH) groups in these sites encouraged us to consider it as the recognition motif.[44−51] However, such an idea is debatable, because all synthetic ion

Received: June 23, 2014
Published: September 9, 2014

dx.doi.org/10.1021/ja506278z | J. Am. Chem. Soc. 2014, 136, 14128−14135

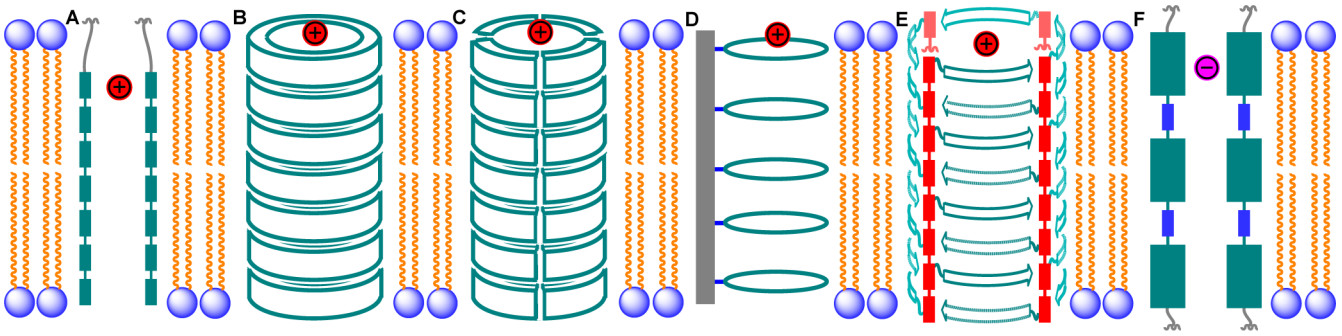

Figure 1. Synthetic ion channel designs with single-file multiple ion-recognition sites: (A) ligand-assembled ion channel based on cation−π interactions, (B) self-assembled cyclic peptide nanotubes based on carbonyl−cation interactions, (C) rosette-type supramolecules based on carbonyl−cation interactions, (D) hydraphile ion channels based on crown ether-cation interactions, (E) barrel-stave ion channels based on either hydroxyl-cation or amino acid side chain-cation interactions, and (F) self-assembled rigid oligo(aromatic diimide) rods based on anion−π interactions.

channels involving a −OH group are cation selective.[37−39,52] In these synthetic channels, recognition of cation by a lone pair of oxygen atoms is responsible for the selectivity.[53] However, a −OH group is also the best known of all hydrogen bond donor groups for recognition of anions[54−56] and, therefore, can in principle be incorporated in the design of an anion selective ion channels, as well.

In order to find a suitable molecule capable of providing multiple −OH groups, mannitol derivatives **1** and **2** (Figure 2A), reported by Sureshan and co-workers,[57] have drawn our attention. In hydrocarbon solvents, these molecules formed transparent gels. On the basis of a variety of experiments, they proposed that the −OH groups facilitate self-assembly of the monomers **M** along one direction to form fibrils $\mathbf{M_n}$ (Figure 2B). These fibrils upon aggregation form fibers, which entangle to form 3D fibrous spaghetti-like networks immobilizing the solvent via capillary force.[57] We predicted that the aggregation of these fibrils $\mathbf{M_n}$ provides a face-to-face assembly, $\mathbf{M_{n,2}}$, which further expands to the fibers. The face-to-face assembled $\mathbf{M_{n,2}}$ aggregate is favorable in either gel or crystalline state. Therefore, it should have negligible internal space. However, when present in the lipid membrane, the fibrils would undergo self-assembly to form nanotubular structures $\mathbf{M_{n,3}}$, $\mathbf{M_{n,4}}$, etc. with definite space for transporting ions (Figure 2B). Overall, each nanotubular structure can also be viewed as layers of supramolecular rosettes formed by either three or four units of **M**, and each rosette would provide a recognition site for an anion A^- via multivalent O−H···A^- hydrogen-bonding interactions. Transport of anion can be predicted through the nanotubular structure, facilitated by the movement of an anion from one rosette to the next in single-file. Cyclohexyl rings of mannitol **1** would be necessary for better channel formation due to strong van der Waals interactions compared to that of **2**.

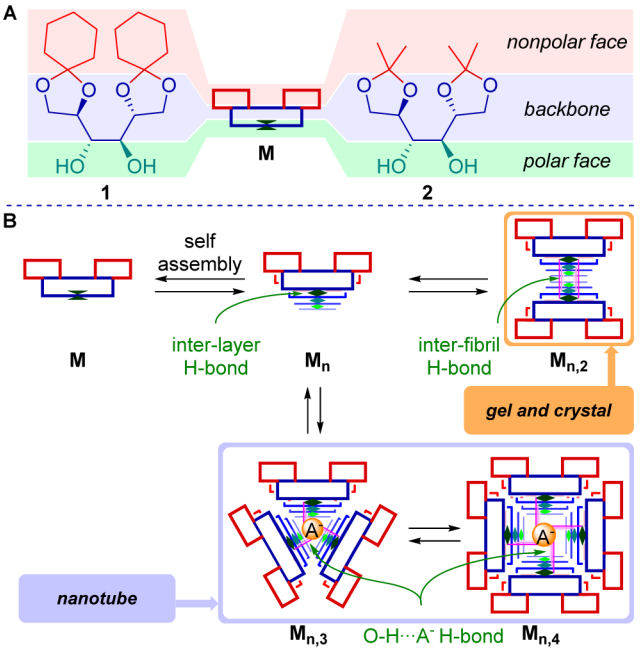

Figure 2. Structures of mannitol derivatives **1** and **2** (A) and schematic representation of self-assembly of these molecules in gel/crystalline state as well as in lipid membrane (B).

2. RESULTS AND DISCUSSION

2.1. Self-Assembly of Mannitol Derivatives 1 and 2 in the Solid State. Mannitol derivative **1** was crystallized from a mixture of acetone and water, and the crystal structure was solved. From the crystal structure, it is evident that both of the −OH groups are involved in a face-to-face hydrogen bond (O3···O3 = 2.73 Å; O4···O4 = 2.76 Å) with identical −OH groups of a neighboring molecule in the "*a*" direction, forming a dimer with a hydrophilic core and hydrophobic periphery (Figure 3A). Such dimers are connected through strong interlayer hydrogen bonds (O3···O4 = 2.76 Å) forming infinite chains along the "*b*" direction. The distance between two molecules along this direction was found to be 5.49 Å (Figure 3A). In other words, the hydrogen bonded infinite fibrils formed along the *b* direction are dimerized along the *a* direction through additional hydrogen bonds. The formation of dimeric fibrils through lateral hydrogen bonds (Figure 3B) suggests the possibility of formation of higher order structures (e.g., trimeric or tetrameric fibrils) through such lateral hydrogen bonds [Figure S3,Supporting Information (SI)]. Also, it is possible to have dynamic interconversion of such higher order structures, especially in response to some stimulus, when the molecules are loosely bound (higher degrees of freedom of motion), unlike in crystals. The presence of an anion can be such stimulus for the formation of such higher order structures ($\mathbf{M_{n,3}}$ or $\mathbf{M_{n,4}}$) in the lipid membranes. In each lateral layer (i.e., either trimeric or tetrameric rosette) of such structure, multivalent O−H···A^- hydrogen bond interactions are feasible for the anion recognition (Figure 2) and the ion can

dx.doi.org/10.1021/ja506278z | J. Am. Chem. Soc. 2014, 136, 14128−14135

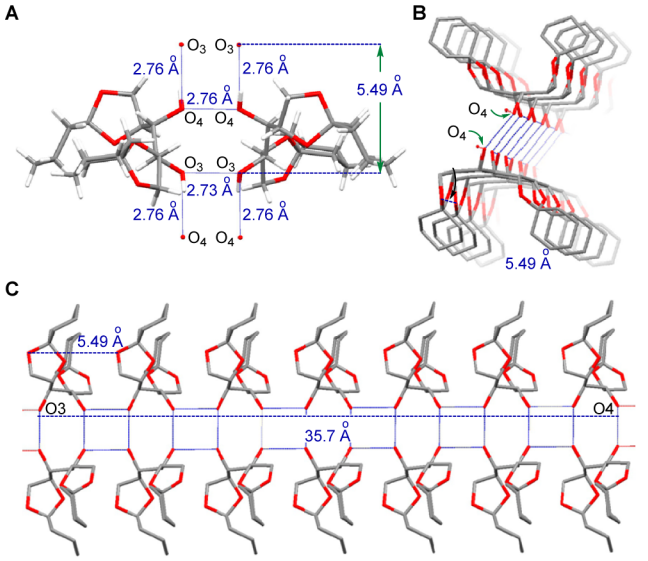

Figure 3. Single crystal structure of **1** showing (A) face-to-face and interlayer hydrogen bonding; top (B) and side views (C) of face-to-face aggregation of ladderlike structures.

hop from one rosette to the next in single-file to facilitate ion permeation. The crystal structure also predicts that a minimum of seven monomer units (i.e., for n = 7, the distance between two exterior O···O = 35.7 Å) is required to span the 37 Å egg yolk phosphatidylcholine (EYPC) bilayer membranes (Figure 3B,C). The crystal structure and packing of **2** are also very similar to those of **1**. However, additional van der Waals interactions between cyclohexyl groups were present in the solid state assembly of **1**.

2.2. Ion-Transporting Activity across Lipid Membranes. The ion-transporting activity of mannitol derivatives **1** and **2** was investigated using 8-hydroxypyrene-1,3,6-trisulfonate (HPTS), a pH-sensitive fluorescent dye (pK_a = 7.2).[58−60] The dye was loaded within EYPC large unilammelar vesicles (LUVs). A pH gradient, ΔpH = 0.8 (pH_{in} = 7.0 and pH_{out} = 7.8) across the EYPC bilayer was applied by addition of NaOH. Upon the addition of a channel-forming compound, the pH gradient collapse via H^+ efflux or OH^- influx leads to an increase in the internal pH of the vesicles, and the process was detected by a change in the fluorescence intensity of HPTS. Complete destruction of the pH gradient was achieved by addition of 10% Triton X-100 (Figure S4, SI). In each ion-transporting experiment, the change of HPTS emission at λ = 510 nm (λ_{ex} = 450 nm) was monitored with time. Compound **1** (20 μM) exhibited high ion-transporting activity, while the derivative **2** (20 μM) was inactive (Figure 4A). Although, the hydrogen-bonded fibril motif is present in the crystal structure of amphiphile **2** (Figure S2, SI), the inactivity could be due to the inability of the molecules of **2** to get embedded in the lipid bilayer due to its less hydrophobic nature and missing van der Waals interactions of the cyclohexyl rings. Also, the hydrophilic nature of **2** may be making it soluble in the aqueous layer. This was evident from its negligible transporting activity even at higher concentration (80 μM). In other words, a proper balance between hydrophobic and hydrophilic features in **1** allows its incorporation in the lipid layer. Self-assembly of **1** in the lipid membranes is facilitated by the network of hydrogen-bonding interactions and van der Waals interactions of cyclohexyl rings.

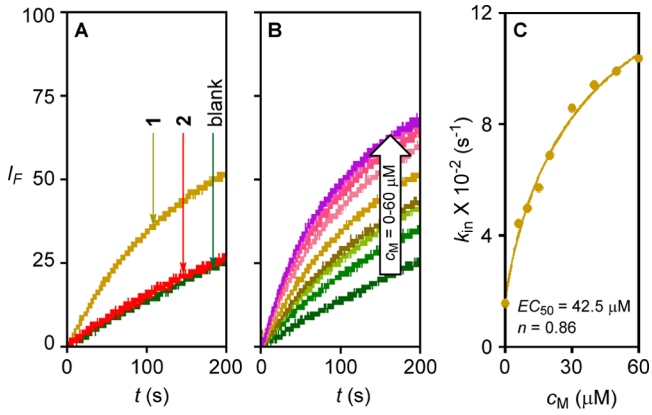

Figure 4. Comparison of ion-transporting activity of mannitol derivatives **1** (20 μM) and **2** (20 μM) in EYPC vesicle, presented as normalized emission intensity (I_F) as a function of time (t) (A). Concentration profile (B) and Hill plot of **1** (C).

A detailed examination of the ion-transporting activity of compound **1** was then carried out by varying its concentrations from 0 to 60 μM (Figure 4B). Pseudo-first-order transport kinetics was observed for the compound. Rate constant (k_{obs}) values were plotted against respective monomer concentration (c_M) values (Figure 4C), and Hill analyses were performed by using eq 1[36,61,62]

$$k_{obs} = k_0 + k_{max}c_M{}^n/(c_M{}^n + EC_{50}{}^n) \quad (1)$$

where k_0 is the rate constant for the blank measurement, EC_{50} is the "effective" monomer concentration of each conjugate needed to reach 50% of the maximum activity (k_{max}), and n is the Hill coefficient, which reveals the stoichiometry of the transport process. From the Hill analysis, EC_{50} = 42.5 μM and n = 0.9 were calculated, which indicates a thermodynamically favorable self-assembly of **1**, which appears as monomers during permeation into the lipid membranes.

2.3. Ion Selectivity Studies by Vesicle Assays. The transporting activity of **1** encouraged us to investigate its ion selectivity and the mechanism of ion transport. At first, the transporting activity was evaluated in the presence of a proton transporter, carbonyl cyanide-4-(trifluoromethoxy)-phenylhydrazone (FCCP) to identify whether a H^+/M^+ antiport (M^+ = alkali metal cation) or OH^-/A^- (A^- = monovalent anion) antiport mechanism is dominant through the ion channel (Figure 5A). FCCP allows selective efflux of H^+

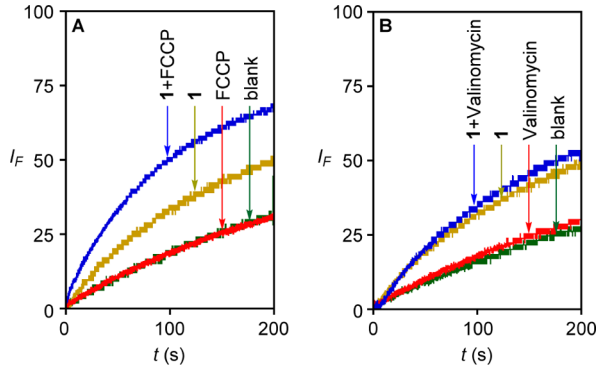

Figure 5. Ion transport activity of **1** (20 μM) determined in the absence and presence of FCCP (A). Ion transport activity of **1** determined in the absence and presence of valinomycin (B).

dx.doi.org/10.1021/ja506278z | J. Am. Chem. Soc. 2014, 136, 14128−14135

ion from the intravesicular water pool to the extravesicular bulk water when a pH gradient is applied across the membrane.[63] Under the applied pH gradient, FCCP (5 μM) exhibited negligible ion transport (Figure 5A). On the other hand, the transporting activity of **1** enhanced by approximately 2-fold when studied in the presence of FCCP, indicating the cooperative effect of **1** and FCCP. From these data, a faster OH^-/A^- exchange compared to H^+/M^+ antiport across the EYPC membrane was confirmed for mannitol derivative **1**. This data is in accordance with our prediction of anion recognition within the channel structure.

A further comparison of transport rate between OH^- and Cl^- was carried out with the help of valinomycin, a K^+ ion selective carrier.[64] In this assay (Figure 5B), a Na^+ versus K^+ gradient was applied between the interior and exterior of EYPC vesicles. Influx of K^+ ion by valinomycin is expected to be accompanied by the OH^-/Cl^- influx to maintain the charge equality. Valinomycin (1 pM) alone did not display any transporting ability (Figure 5B). Fluorescence enhancement of HPTS was nearly similar when **1** (20 μM) was tested in the absence and presence of valinomycin. These results confirm preferential transport of Cl^- ion through the channel formed by **1** over OH^- ion. This effect implies that the channel formed by **1** acts as an OH^-/Cl^- exchanger with a faster rate of Cl^- ion transport compared to OH^- (i.e., a $Cl^- > OH^-$ selectivity).

Anion transport across the channel formed by **1** encouraged us to determine the selectivity sequences caused by isoosmolar Cl^- (intravesicular) to monovalent anion A^- (extravesicular) exchange. Upon variation of extravesicular anions, a selectivity topology, $Cl^- > NO_3^- > Br^- > SCN^- > ClO_4^- \geq I^- > OAc^- \geq F^-$, was determined for **1** (Figure 6A). To rationalize the

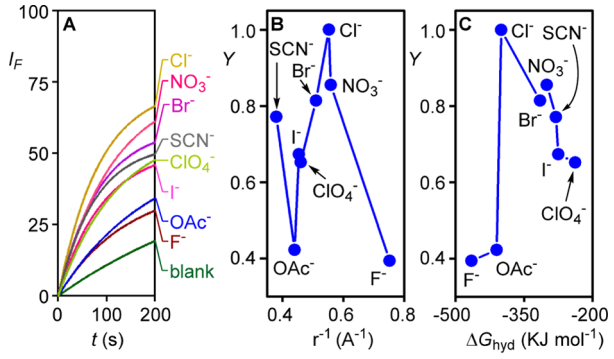

Figure 6. Anion selectivity of **1** determined with the HPTS assay with intravesicular Cl^- ion and varied external anions A^-. Anion selectivity presented as fractional emission I_F as a function of time (A), fractional activity Y (relative to Cl^-) as a function of the reciprocal anion radius (B), and fractional activity Y (relative to Cl^-) as a function of the anion hydration energy (C).

observation, the dependence of the fractional activity Y on the reciprocal anion radius (Figure 6B) or the anion hydration energy (Figure 6C) was plotted. Poor transport of weakly basic anion such as OAc^- or F^- suggested that the origin of the derived Cl^- selectivity is mainly energetic, and contribution from anionic radii ($OAc^- \gg F^-$) can be excluded. The selectivity of mannitol derivative **1**, derived from HPTS assays, decreased with increasing halide radius (i.e., $Cl^- > Br^- > I^-$). This halide topology is unusually rare (either of halide V, VI, or VII Hofmeiser series)[8,9,42,66] and opposite to the common, dehydration-dominated Hofmeiser series or halide I sequence. Binding of Cl^- ion by O–H···Cl^- interactions along the nanotube is responsible for the exceptional selectivity and is supported by the Eisenman theory.[65,66] Variation of external cations ($M^+ = Li^+$, Na^+, K^+, Rb^+, and Cs^+) did not provide any difference in ion-transporting behavior, which further establishes that the rosette channel is specific to only anions (Figure S9, SI).

2.4. Mass Spectrometric Evidence of Anion Binding. Electrospray ionization mass spectrometric (ESI-MS) studies were carried out to obtain direct evidence of anion recognition by mannitol **1** because the technique is suitable to deliver the direct experimental evidence of weak supramolecular interactions.[67,68] Samples were prepared in acetonitrile by mixing **1** with Me_4NCl in 2:1 and 3:1 molar ratios and then electrosprayed under as mild as possible ionization conditions. When data were recorded from the 2:1 molar solution, formation of the $\mathbf{1}_2 \cdot Cl^-$ adduct was detected (Figure S10, SI). On the other hand, data recorded from the 3:1 molar solution provided a weak signal of $\mathbf{1}_3 \cdot Cl^-$ adduct in addition to the dominant $\mathbf{1}_2 \cdot Cl^-$ adduct (Figures S11 and S12, SI). These results support Cl^- ion recognition by either two or three units of **1**, even in the gas phase via O–H···Cl^- interactions.

2.5. Single-Channel Conductance Measurements. Mannitol derivative **1** readily formed a channel in the bilayer lipid membrane (BLM), when added to the cis chamber. Distinct single-channel opening and closing events were observed at different holding potentials (Figure 7A,B). Single-

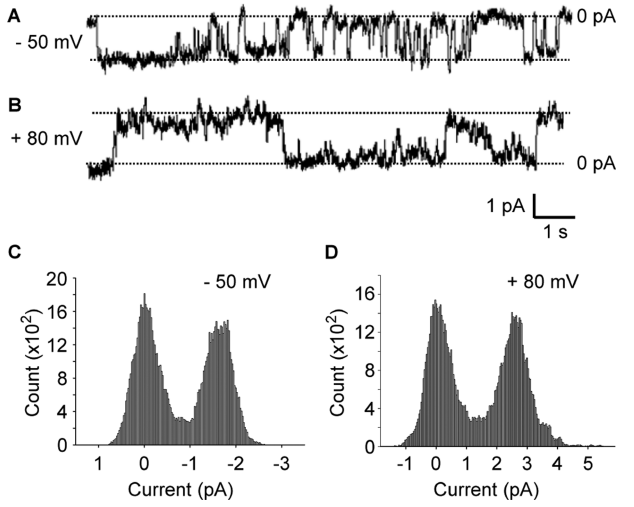

Figure 7. Single-channel current traces recorded at −50 mV (A) and +80 mV (B) holding potentials in 1 M symmetrical KCl solution. 0 pA at the right-hand side indicates the baseline current. The main conductance state is indicated by two dotted lines. All point histograms generated from the corresponding current traces at −50 mV (C) and +80 mV (D), respectively. The conductance of the main open state is 38.1 ± 3 pS (calculated from four independent experiments).

channel conductance, calculated from the all-point histogram (Figure 7C,D) appeared to be about 38.1 ± 3 pS (in 1 M KCl). A current–voltage relationship plot (I–V plot) derived from the BLM, containing multiple channels, is shown in Figure 8. The I–V plot followed an ohmic relation with symmetrical currents at negative and positive polarity. The I–V plot was generated in asymmetrical bathing solution with a KCl gradient (1 M in cis:0.5 M in trans) to check the ion selectivity. As shown in Figure 8, the reversal potential is −20 mV, which is close to the theoretically derived equilibrium potential of Cl^-

dx.doi.org/10.1021/ja506278z | J. Am. Chem. Soc. 2014, 136, 14128–14135

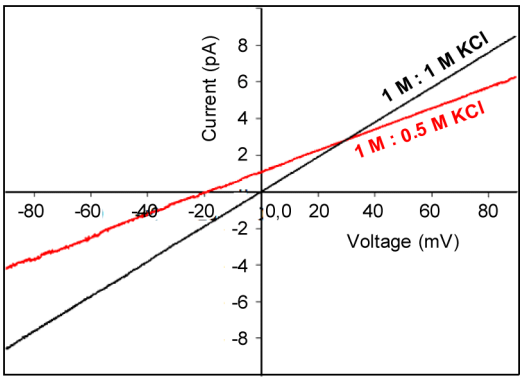

Figure 8. *I*–*V* plot using a voltage ramp (−90 mV to +90 mV) in 1 M symmetrical KCl solution (black line) and in 1 M:0.5 M KCl gradient (red line).

(−17.8 mV), using the Nernst equation. It confirms that the conducting ion is Cl^-.

The diameter of the artificial ion channel can also be determined as 3.06 Å by BLM measurements by applying eq 2

$$1/g = (l + \pi d/4)(4\rho/\pi d^2) \quad (2)$$

where g = corrected conductance (obtained by multiplying measured conductance with the Sansom's correction factor), l = length of the ion channel (34 Å), and ρ = resistivity of the recording solution (ρ = 9.44 Ω·cm).

2.6. Molecular Model of Ion Channel and Free Energy Profile of Ion Transport. Molecular level insight was acquired from further computational study of the ion channel formation and passage of Cl^- ion. To create the model of the ion channel, the monomer **1** was first optimized quantum mechanically using Gaussian 09[69] software with wB97X-D[70] functional and 6-31g(d) basis set. Further, we constructed a trimeric configuration from the optimized monomers first. This was further optimized by using the same functional and basis set (Figure S13, SI). This optimized trimer was then used for the channel construction (3 × 3 = three columns and three rows) by placing three trimers together followed by further optimization of the entire channel (nine monomeric units) semiempirically at the PM6 level using MOPAC2009[71] (Figure S14A, SI). Further optimization of the trimeric channel was done with Cl^- incorporated as well (Figure S14B, SI). We also built a channel consisting of 12 monomeric units (4 × 3 = four columns and three rows) placing four trimers together, followed by optimization of the whole channel with (Figure S15B, SI) and without (Figure S15A, SI) a Br^- ion incorporated. The diameter of the 3 × 3 channel model was calculated to be 3.23 Å, whereas the diameter of the 4 × 3 channel was 4.60 Å. The diameter of the model-generated 3 × 3 channel (3.23 Å) agrees well with the channel diameter (3.06 Å) obtained from conductance measurement. Therefore, we proceeded with the 3 × 3 channel to construct a 3 × 5 channel model and optimized it using the molecular mechanical force field of the monomer (described below). The structure of the optimized 3 × 5 channel with Cl^- ion is shown in Figure 9.

After constructing the channel with the anion, we embedded it in a pre-equilibrated 1,2-dipalmitoyl-*sn*-phosphocholine (DPPC)/water lipid bilayer[72] maintaining the ratio of the number of water molecules to the number of lipid molecules to be ∼28. The system consists of 94 lipid molecules and 2658 water molecules. GROMOS-53a6 united atom force field[73] was

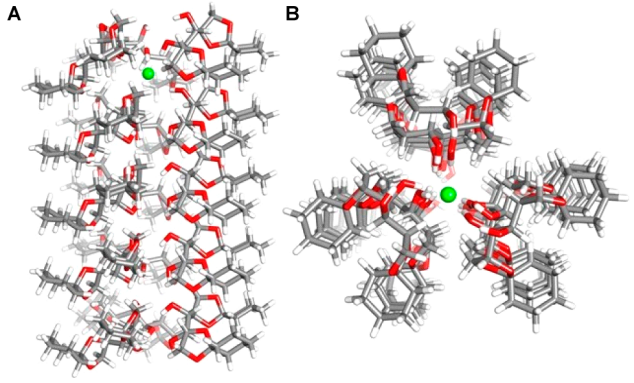

Figure 9. Lateral (A) and top (B) view of the optimized structures of ion channels containing 3 × 5 monomers with Cl^- ion.

used for DPPC molecules and SPC model[74] was used for water. The box dimension is 6.18 × 6.18 × 5.89 nm^3. One Na^+ ion was added to neutralize the system. The system was minimized and equilibrated for 500 ps restraining the channel. The equilibrated system is shown in Figure 10A.

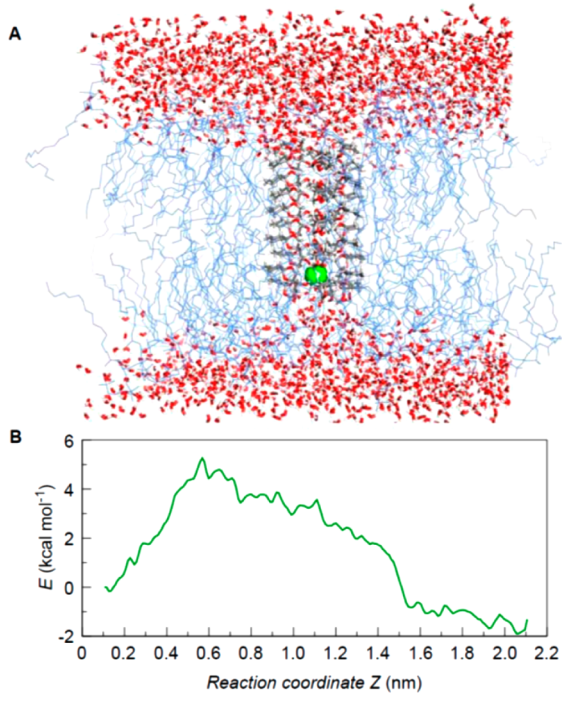

Figure 10. Equilibrated channel–DPPC/water system (A), and free energy profile of a Cl^- ion while moving through the channel lumen (B).

With the constructed and embedded channel, we performed umbrella sampling to calculate the free energy for the passage of the chloride ion through the channel. We used GROMACS[75] molecular dynamics software to carry out all the simulations. General AMBER force-field (GAFF)[76] for monomer was calculated by performing a quantum calculation using Hartree–Fock theory and the 6-31G(d) basis set using Gaussian 03.[77] AmberTools[78] was used to construct the topology and RESP charges. The coordinates and topology were converted to GROMACS format using the amb2gmx.pl program.[79]

dx.doi.org/10.1021/ja506278z | J. Am. Chem. Soc. 2014, 136, 14128–14135

To calculate the free energy of the ion movement along the channel, we performed a series of simulations with an external harmonic potential $[1/2k(Z - Z_0)^2$, where k is the force constant (25 kcal/mol) and Z_0 equilibrium point of the potential] to accelerate sampling of the barrier region (known as umbrella sampling simulations).[80] The distance (Z) between the reference group and the chloride ion serves as the reaction coordinate. We have considered the center of mass of the bottom layer of the channel as the reference group. We performed 65 simulations by placing the center of the umbrella potential Z_0 at a separation of 0.3 Å. For each simulation, we started with the same initial configuration (Figure 9), however, placing Cl^- closest to Z_0. In each simulation, the system was simulated for 1.5 ns at constant temperature (300 K) and constant pressure (1 bar) using the Nose–Hoover[81] thermostat with a coupling constant of 0.5 ps and the Parrinello–Rahman[82] barostat with a coupling constant of 1 ps. The time step of each simulation was taken as 2 fs. Electrostatic interaction was treated using particle mesh Ewald[83] (PME) with a cutoff at 12 Å, and the van der Waals (vdW) cutoff was taken at 12 Å. The GROMACS analysis program g_wham[84] was used to calculate the free energy using the final 1 ns simulation.

The free energy profile along the channel is shown in Figure 10B. The convergence in the free energy profile is shown in Figure S16 (SI). From the free energy profile we conclude that the barrier to cross the channel is ∼6.5 kcal/mol, which indicates that the rate of chloride ion passing will be in the range from ∼10 ns to submicroseconds. The free energy profile is almost symmetric on both sides. The origin of the barrier is entropic because of the less mobility of the anion in the channel compared to the water layer. Moreover, less accessibility to hydrogen bonding to water also contributes to the barrier.

To understand the molecular mechanism of Cl^- ion transport across the membrane, we have calculated the average number of hydrogen bonds formed by the −OH groups of each mannitol derivative with Cl^- ion from the above 65 simulations.

Figure 11 shows the contour plot of the average value of the hydrogen bonds formed between the Cl^- and the −OH group contributed by the mannitol derivatives at different layers along the reaction coordinate Z. As Z increases, Cl^- ion moves along the channel by breaking the multivalent O–H···Cl^- interaction in one layer and forming the same in the next, thus indicating that the transport is happening via transfer of hydrogen bonds from one rosette to the next. We observe that a maximum of four hydrogen bonds are made at any time. We have also noticed that the molecules are rather flexible, even in the bilayer. However, each time Cl^- ion is surrounded by some monomers it primarily forms hydrogen bonds to chloride through the hydroxyl group. In some cases, hydrogen bonds become fewer where some water molecules insert into the layer and contribute to hydrogen bonding. However, we do not see any loss of hydrogen bonds along the path, indicating that the monomers are flexible, and therefore, all along the channel they contribute to hydrogen bonding to the ion, defining a hopping mechanism, at least in this case.

Whenever the Cl^- ion is in between the two consecutive rosettes of the channel, it forms a hydrogen bond with both rosettes, providing energetic stability. When the ion crosses one rosette, it comes close to the oxygen atoms of the hydroxyl groups, which makes the system go through a barrier. The barrier is so small that the Cl^- ion can hop from one low-energy state to another low-energy state.

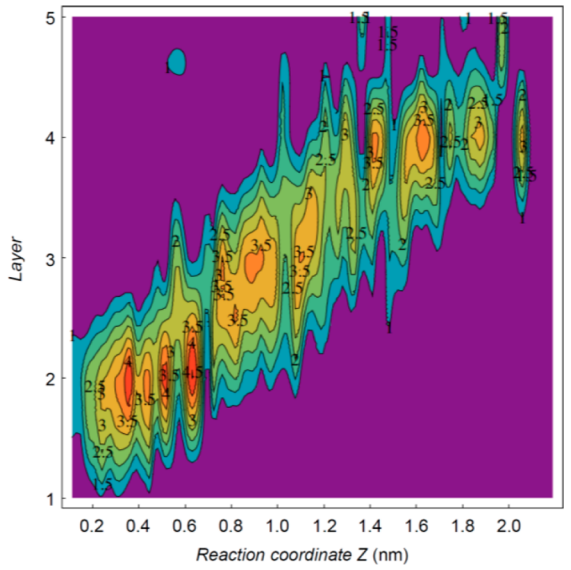

Figure 11. 2-D contour plot of Cl^- transport across the channel. The average number of hydrogen bonds to the Cl^- ion along the channel is shown.

3. CONCLUSION

In summary, artificial ion channels were designed from diketal-protected mannitols **1** and **2**. Formation of a supramolecular ion channel was proposed in the lipid membranes via rosette-type self-assembly of either three or four units of the monomer and a subsequent single-file arrangement of these rosettes via hydrogen-bonding interactions. Evidence of such hydrogen-bonding interactions was obtained from the crystal structure of **1**, and subsequently, the possibility of anion recognition within the channel was predicted. The derivative **1**, containing cyclohexylidene groups, displayed ion-transporting activity (EC_{50} = 42.5 μM), while derivative **2**, with isopropylidene groups, was inactive. A proper balance between hydrophobicity and hydrophilicity favored the incorporation of the ion channel formed by **1** into the lipid bilayer membranes. Fluorescence-based vesicle assay and planar bilayer conductance measurements confirmed selective transport of anions through the active channel. The observed selectivity was explained by the multivalent O–H···A^- hydrogen-bonding interaction of an anion (A^-) with free −OH groups of each rosette. Experimental evidence of anion recognition by **1** was also provided by mass spectrometry. Molecular dynamics (MD) simulations indicate that the trimeric channel with internal diameter 3.23 Å is more feasible, compared with the experimental value 3.06 Å obtained from single-channel conductance measurements. It also indicates that the channel molecules present in a rosette surround and interact with the Cl^- ion via multiple O–H···Cl^- hydrogen bonds and the ion is then passed to the next layer of molecules, ensuring a relay mechanism during transport.

■ ASSOCIATED CONTENT

Ⓢ Supporting Information

General methods, physical measurements, synthesis, single-crystal X-ray diffraction studies, ion transport across spherical lipid bilayer membranes, mass spectrometric studies for anion recognition, planar bilayer conductance measurements, molecular modeling studies, references, and crystallographic data in

dx.doi.org/10.1021/ja506278z | J. Am. Chem. Soc. 2014, 136, 14128–14135

CIF format for compounds **1** and **2**. This material is available free of charge via the Internet at http://pubs.acs.org.

AUTHOR INFORMATION

Corresponding Authors

amal@iitm.ac.in
arnab.mukherjee@iiserpune.ac.in
ptalukdar@iiserpune.ac.in

Notes

The authors declare no competing financial interest.

ACKNOWLEDGMENTS

This work is supported by Department of Science and Technology (DST), New Delhi, India, under the following grants: SR/S1/OC-65/2012, SB/S1/PC-39/2012, and SR/NM/NS-42/2009. T.S. thanks UGC (University Grant Commission), India, for research fellowships. A.M. thanks Dr. Sudip Roy (NCL Pune) for providing bilayer configuration and the corresponding force field. K.M.S. thanks Department of Science and Technology (DST), New Delhi, India, for the Ramanujan fellowship, Swarnajayanti fellowship, and funding.

REFERENCES

(1) Mosgaard, L. D.; Heimburg, T. *Acc. Chem. Res.* **2013**, *46*, 2966.
(2) Hladky, S. B.; Haydon, D. A. Ion Movement in Gramicidin Channels. In *Current Topics in Membranes and Transport*; Bronner, F., Ed.; Academic Press, New York, 1984; Vol. *21*, pp 327−372.
(3) Song, L.; Hobaugh, M. R.; Shustak, C.; Cheley, S.; Bayley, H.; Gouaux, J. E. *Science* **1996**, *274*, 1859.
(4) Legutko, B.; Staufenbiel, M.; Krieglstein, K. *Int. J. Dev. Neurosci.* **1998**, *16*, 347.
(5) Chiu, S. Y.; Wilson, G. F. *J. Physiol.* **1989**, *408*, 199.
(6) DeCoursey, T. E.; Chandy, K. G.; Gupta, S.; Cahalan, M. D. *Nature* **1984**, *307*, 465.
(7) Lange, K. *J. Cell. Physiol.* **2000**, *185*, 21.
(8) Hille, B.; Schwarz, W. *J. Gen. Physiol.* **1978**, *72*, 409.
(9) Miller, C. *J. Gen. Physiol.* **1999**, *113*, 783.
(10) Hille, B. *Ionic Channels of Excitable Membranes*, 3rd ed.; Sinauer Associates: Sunderland, MA, 2001.
(11) Keramidas, A.; Moorhouse, A. J.; Schofield, P. R.; Barry, P. H. *Prog. Biophys. Mol. Bio.* **2004**, *86*, 161.
(12) Gouaux, E.; MacKinnon, R. *Science* **2005**, *310*, 1461.
(13) Corry, B.; Chung, S. H. *Cell. Mol. Life Sci.* **2006**, *63*, 301.
(14) Tsien, R. W.; Hess, P.; McCleskey, E. W.; Rosenberg, R. L. *Annu. Rev. Biophys. Biophys. Chem.* **1987**, *16*, 265.
(15) Chen, W.-H.; Nishikawa, M.; Tan, S.-D.; Yamamura, M.; Satake, A.; Kobuke, Y. *Chem. Commun.* **2004**, 872.
(16) Sisson, A. L.; Shah, M. R.; Bhosale, S.; Matile, S. *Chem. Soc. Rev.* **2006**, *35*, 1269.
(17) Matile, S.; Som, A.; Sorde, N. *Tetrahedron* **2004**, *60*, 6405.
(18) Chen, W.-H.; Nishikawa, M.; Tan, S.-D.; Yamamura, M.; Satake, A.; Kobuke, Y. *Chem. Commun.* **2004**, 872.
(19) Chui Jonathan, K. W.; Fyles, T. M. *Org. Biomol. Chem.* **2014**, *12*, 3622.
(20) Madhavan, N.; Robert, E. C.; Gin, M. S. *Angew. Chem., Int. Ed.* **2005**, *44*, 7584.
(21) Saha, T.; Roy, A.; Gening, M. L.; Titov, D. V.; Gerbst, A. G.; Tsvetkov, Y. E.; Nifantiev, N. E.; Talukdar, P. *Chem. Commun.* **2014**, *50*, 5514.
(22) Tedesco, M. M.; Ghebremariam, B.; Sakai, N.; Matile, S. *Angew. Chem., Int. Ed.* **1999**, *38*, 540.
(23) Ishida, H.; Qi, Z.; Sokabe, M.; Donowaki, K.; Inoue, Y. *J. Org. Chem.* **2001**, *66*, 2978.
(24) Bong, D. T.; Clark, T. D.; Granja, J. R.; Ghadiri, M. R. *Angew. Chem., Int. Ed.* **2001**, *40*, 988.
(25) Sánchez-Quesada, J.; Isler, M. P.; Ghadiri, M. R. *J. Am. Chem. Soc.* **2002**, *124*, 10004.
(26) Fernandez-Lopez, S.; Kim, H.-S.; Choi, E. C.; Delgado, M.; Granja, J. R.; Khasanov, A.; Kraehenbuehl, K.; Long, G.; Weinberger, D. A.; Wilcoxen, K. M.; Ghadiri, M. R. *Nature* **2001**, *412*, 452.
(27) Clark, T. D.; Buehler, L. K.; Ghadiri, M. R. *J. Am. Chem. Soc.* **1998**, *120*, 651.
(28) Ghadiri, M. R.; Granja, J. R.; Buehler, L. K. *Nature* **1994**, *369*, 301.
(29) Forman, S. L.; Fettinger, J. C.; Pieraccini, S.; Gottarelli, G.; Davis, J. T. *J. Am. Chem. Soc.* **2000**, *122*, 4060.
(30) Sakai, N.; Kamikawa, Y.; Nishii, M.; Matsuoka, T.; Kato, T.; Matile, S. *J. Am. Chem. Soc.* **2006**, *128*, 2218.
(31) Hennig, A.; Matile, S. *Chirality* **2008**, *20*, 932.
(32) Pedersen, C. J. *J. Am. Chem. Soc.* **1967**, *89*, 2495.
(33) Pedersen, C. J. *J. Am. Chem. Soc.* **1967**, *89*, 7017.
(34) Winum, J.-Y.; Matile, S. *J. Am. Chem. Soc.* **1999**, *121*, 7961.
(35) Cazacu, A.; Tong, C.; van der Lee, A.; Fyles, T. M.; Barboiu, M. *J. Am. Chem. Soc.* **2006**, *128*, 9541.
(36) Boudreault, P.-L.; Voyer, N. *Org. Biomol. Chem.* **2007**, *5*, 1459.
(37) Sakai, N.; Brennan, K. C.; Weiss, L. A.; Matile, S. *J. Am. Chem. Soc.* **1997**, *119*, 8726.
(38) Weiss, L. A.; Sakai, N.; Ghebremariam, B.; Ni, C.; Matile, S. *J. Am. Chem. Soc.* **1997**, *119*, 12142.
(39) Ni, C.; Matile, S. *Chem. Commun.* **1998**, 755.
(40) Sakai, N.; Majumdar, N.; Matile, S. *J. Am. Chem. Soc.* **1999**, *121*, 4294.
(41) Gorteau, V.; Bollot, G.; Mareda, J.; Perez-Velasco, A.; Matile, S. *J. Am. Chem. Soc.* **2006**, *128*, 14788.
(42) Gorteau, V.; Bollot, G.; Mareda, J.; Matile, S. *Org. Biomol. Chem.* **2007**, *5*, 3000.
(43) Perez-Velasco, A.; Gorteau, V.; Matile, S. *Angew. Chem., Int. Ed.* **2008**, *47*, 921.
(44) Wojcik, J. F.; Rohrbach, R. P. *J. Phys. Chem.* **1975**, *79*, 2251.
(45) Pelizzi, N.; Casnati, A.; Ungaro, R. *Chem. Commun.* **1998**, 2607.
(46) Davis, A. P.; Perry, J. J.; Wareham, R. S. *Tetrahedron Lett.* **1998**, *39*, 4569.
(47) Hayashida, O.; Kato, M.; Akagi, K.; Aoyama, Y. *J. Am. Chem. Soc.* **1999**, *121*, 11597.
(48) Arduini, A.; Giorgi, G.; Pochini, A.; Secchi, A.; Ugozzoli, F. *J. Org. Chem.* **2001**, *66*, 8302.
(49) Miyaji, H.; Sessler, J. L. *Angew. Chem., Int. Ed.* **2001**, *40*, 154.
(50) Tong, H.; Zhou, G.; Wang, L.; Jing, X.; Wang, F.; Zhang, J. *Tetrahedron Lett.* **2003**, *44*, 131.
(51) Sessler, J. L.; Gale, P. A.; Cho, W.-S. In *Anion Receptor Chemistry (Monographs in Supramolecular Chemistry)*; Stoddart, J. F., Ed.; RSC: Cambridge, 2006; pp 205−210.
(52) Yamashita, K.; Janout, V.; Bernard, E.; Armstrong, D.; Regen, S. L. *J. Am. Chem. Soc.* **1995**, *117*, 6249.
(53) Koenig, K. E.; Lein, G. M.; Stuckler, P.; Kaneda, T.; Cram, D. J. *J. Am. Chem. Soc.* **1979**, *101*, 3553.
(54) Clare, J. P.; Ayling, A. J.; Joos, J.-B.; Sisson, A. L.; Magro, G.; Pérez-Payán, M. N.; Lambert, T. N.; Shukla, R.; Smith, B. D.; Davis, A. P. *J. Am. Chem. Soc.* **2005**, *127*, 10739.
(55) Davis, A. P.; Gilmer, J. F.; Perry, J. J. *Angew. Chem., Int. Ed.* **1996**, *35*, 1312.
(56) Ashokkumar, P.; Ramakrishnan, V. T.; Ramamurthy, P. *ChemPhysChem* **2011**, *12*, 389.
(57) Vidyasagar, A.; Handore, K.; Sureshan, K. M. *Angew. Chem., Int. Ed.* **2011**, *50*, 8021.
(58) Sakai, N.; Matile, S. *J. Phys. Org. Chem.* **2006**, *19*, 452.
(59) Talukdar, P.; Bollot, G.; Mareda, J.; Sakai, N.; Matile, S. *J. Am. Chem. Soc.* **2005**, *127*, 6528.
(60) Sakai, N.; Matile, S. *J. Am. Chem. Soc.* **2003**, *125*, 14348.
(61) Qu, Z.; Hartzell, H. C. *J. Gen. Physiol.* **2000**, *116*, 825.
(62) Sakai, N.; Gerard, D.; Matile, S. *J. Am. Chem. Soc.* **2001**, *123*, 2517.
(63) Benz, R.; McLaughlin, S. *Biophys. J.* **1983**, *41*, 381.
(64) Rose, L.; Jenkins, A. T. A. *Bioelectrochemistry* **2007**, *70*, 387.

(65) Wright, E. M.; Diamond, J. M. *Physiol. Rev.* **1977**, *57*, 109.
(66) Eisenman, G.; Horn, R. *J. Membr. Biol.* **1983**, *76*, 197.
(67) Weimann, D. P.; Kogej, M.; Schalley, C. A. Mass Spectrometry and Gas Phase Chemistry of Supramolecules. In *Analytical Methods in Supramolecular Chemistry*, 2nd ed.; Schalley, C. A., Ed.; Wiley-VCH: Weinheim, 2012; Vol. *1*, pp 129−196.
(68) Dawson, R. E.; Hennig, A.; Weimann, D. P.; Emery, D.; Ravikumar, V.; Montenegro, J.; Takeuchi, T.; Gabutti, S.; Mayor, M.; Mareda, J.; Schalley, C. A.; Matile, S. *Nat. Chem.* **2010**, *2*, 533.
(69) Frisch, M. J.; et al. *Gaussian 09*, Revision B.01, Gaussian, Inc., Wallingford CT, 2010.
(70) Chai, J.-D.; Head-Gordon, M. *Phys. Chem. Chem. Phys.* **2008**, *10*, 6615.
(71) Stewart J. J. P. *MOPAC2009*, Version 11.366L; Stewart Computational Chemistry, Colorado Springs, CO, 2009; http://OpenMOPAC.net.
(72) Pandey, P. R.; Roy, S. *J. Phys. Chem. B* **2011**, *115*, 3155.
(73) Oostenbrink, C.; Villa, A.; Mark, A. E.; van Gunsteren, W. F. *J. Comput. Chem.* **2004**, *25*, 1656.
(74) Berendsen, H. J. C.; Postma, J. P. M.; van Gunsteren, W. F.; Hermans, J. Interaction Models for Water in Relation to Protein Hydration. In *Intermolecular Forces*; Pullman, B., Ed.; Reidel: Dordrecht, 1981; pp 331−342.
(75) Hess, B.; Kutzner, C.; van der Spoel, D.; Lindahl, E. *J. Chem. Theory Comput.* **2008**, *4*, 435.
(76) Wang, J.; Wolf, R. M.; Caldwell, J. W.; Kollman, P. A.; Case, D. A. *J. Comput. Chem.* **2004**, *25*, 1157.
(77) Frisch, M. J. et al.. *Gaussian 03*, Revision E.01; Gaussian, Inc., Wallingford CT, 2004.
(78) Case, D. A.; Cheatham, T. E., III; Darden, T.; Gohlke, H.; Luo, R.; Merz, K. M., Jr.; Onufriev, A.; Simmerling, C.; Wang, B.; Woods, R. J. *J. Comput. Chem.* **2005**, *26*, 1668.
(79) Sorin, E. J.; Pande, V. S. *Biophys. J.* **2005**, *88*, 2472.
(80) Torrie, G. M.; Valleau, J. P. *Chem. Phys. Lett.* **1974**, *28*, 578.
(81) Nose, S. *Mol. Phys.* **1984**, *52*, 255.
(82) Parrinello, M.; Rahman, A. *J. Appl. Phys.* **1981**, *52*, 7182.
(83) Darden, T.; York, D.; Pedersen, L. *J. Chem. Phys.* **1993**, *98*, 10089.
(84) Hub, J. S.; de Groot, B. L.; van der Spoel, D. *J. Chem. Theory Comput.* **2010**, *6*, 3713.